Molecular Crystals and Liquid Crystals Science and Technology. Section A. Molecular Crystals and Liquid Crystals

Publication details, including instructions for authors and subscription information:
http://www.tandfonline.com/loi/gmcl19

Director Structures of Cholesteric Diffraction Gratings

S. V. Shiyanovskii [a], D. Voloschenko [a], T. Ishikawa [a] & O. D. Lavrentovich [a]

[a] Chemical Physics Interdisciplinary Program and Liquid Crystal Institute, Kent State University, Kent, Ohio, 44242

Version of record first published: 24 Sep 2006

To cite this article: S. V. Shiyanovskii, D. Voloschenko, T. Ishikawa & O. D. Lavrentovich (2001): Director Structures of Cholesteric Diffraction Gratings, Molecular Crystals and Liquid Crystals Science and Technology. Section A. Molecular Crystals and Liquid Crystals, 358:1, 225-236

To link to this article: http://dx.doi.org/10.1080/10587250108028283

Mol. Cryst. and Liq. Cryst., 2001, Vol. 358, pp. 225-236
Reprints available directly from the publisher
Photocopying permitted by license only

Director Structures of Cholesteric Diffraction Gratings

S. V. SHIYANOVSKII*, D. VOLOSCHENKO, T. ISHIKAWA and O. D. LAVRENTOVICH

Chemical Physics Interdisciplinary Program and Liquid Crystal Institute, Kent State University, Kent, Ohio 44242

We study director structures of electrically-controlled cholesteric diffraction gratings (CDG's). The cholesteric liquid crystal (LC) is confined between two transparent non-patterned electrodes with either planar or homeotropic anchoring. In cells with planar alignment, the applied electric field causes reorientation of the initial (zero field) planar state and creates one-dimensionally modulated structures in the plane of the cell. The modulations occur via two distinct scenarios: (I) nucleation and expansion of 'stripes' and (II) undulation of quasinematic layers in the plane normal to the cell's plates. In the cells with homeotropic surface alignment, modulated structures exist without applied voltage. Magnetic field is used to provide uniform orientation of these structures. Confocal microscope studies and computer simulations are carried out to reveal the fine structure of the CDG's.

Keywords: cholesteric liquid crystal; optical diffraction; beam steering; field-controlled grating; computer simulations

1. INTRODUCTION

LC diffraction gratings have certain potential advantages over conventional ruled or holographic gratings. Large birefringence of LC's, a possibility to switch between 'on' and 'off' states using low-

* Electronic mail: svshiyan@lci.kent.edu

voltage electric fields make LC structures attractive for various applications in beam steering, diffractive optics, etc. The optical phased array technology, reviewed by McManamon *et al.*[1], is the most developed concept of the liquid crystal beam steering devices[1-6]. The voltage applied to patterned electrodes produces an inhomogeneous periodic distortion of the director field in a nematic LC and results in the phase-modulated diffraction grating. A deflecting angle of the grating is determined by the distance between adjacent electrodes and by the number of electrodes that produce a required phase profile.

We develop a concept of beam steering based on diffraction properties of the helical structure in cholesteric LC cells that are controlled by the electric field[7-10]. An ideal CDG should represent a uniform one-directional modulation in the plane of the cell. The director modulations originate in the natural tendency of the cholesteric LC to twist. The in-plane uniformity and amplitude of director distortions is achieved by balancing two additional factors: the dielectric coupling and the surface anchoring. The dielectric coupling keeps the twist axis in the plane of the cell, while the surface anchoring (e.g., due to mechanical rubbing of the boundary plates) orients the modulations along one direction in the plane of the cell.

In this work, we review some of the previous studies and present new results for different field-induced textures in cholesteric cells with planar or homeotropic anchoring. The CDG's appear through two different scenarios:[10] (I) nucleation and growth of stripes; (II) barrier-free development of modulations via undulations of quasi-nematic layers in the plane normal to the cell. The internal structure of the modulated states is revealed by polarizing and confocal microscopy as well as by computer simulations.

The article is organized as follows. Mathematical basis of computer simulations is given in Section 2. The program simulates two- or three-dimensionally-distorted nematic and cholesteric slabs, taking into account different elastic constants, finite anchoring and inhomogeneous electric field effects. When the simulated director field is periodic, a special scaling procedure finds a self-consistent period to make sure that the periodicity is not affected by the finite size of the computational cell. Section 3 describes experimental techniques. Experimental and simulated results are presented in section 4.

2. MATHEMATICAL BASIS FOR COMPUTER SIMULATIONS OF EQUILIBRIUM STRUCTURES

The equilibrium director field is found by minimizing the free energy functional, which is a sum of the Frank-Oseen bulk energy and the surface anchoring energy. Usually LC's with large dielectric anisotropy are used in experiments and inhomogeneity of the electric field can be significant even when the electrodes are homogeneous. In this work we find the electric potential $V(\mathbf{r})$ inside the cell self-consistently. The Frank-Oseen functional is also supplemented by the divergence (saddle-splay) elastic K_{24} term:

$$F_{FO} = \int \left[\begin{array}{l} \frac{K_{11}}{2}(\mathrm{div}\,\mathbf{n})^2 + \frac{K_{22}}{2}(\mathbf{n}\,\mathrm{curl}\,\mathbf{n} - q)^2 + \frac{K_{33}}{2}[\mathbf{n}\times\mathrm{curl}\,\mathbf{n}]^2 - \\ - K_{24}\,\mathrm{div}(\mathbf{n}\,\mathrm{div}\,\mathbf{n} + \mathbf{n}\times\mathrm{curl}\,\mathbf{n}) - \frac{\varepsilon_0}{2}(\nabla V\cdot\hat{\varepsilon}\cdot\nabla V) \end{array} \right] d^3\mathbf{r}, \qquad (1)$$

where K_{11} (K_{22}, K_{33}) is the splay (twist, bend) elastic constant, $\hat{\varepsilon}$ is the relative dielectric tensor with components dependent on the director orientation:

$$\varepsilon_{ij} = \varepsilon_{\perp}\,\delta_{ij} + \varepsilon_a\,n_i\,n_j\,. \qquad (2)$$

Variation of F_{FO} with respect to the potential V inside the cell gives the Maxwell equation:

$$\frac{\delta F_{FO}}{\delta V} = \mathrm{div}(\varepsilon_0\varepsilon\nabla V) = 0\,. \qquad (3)$$

The surface anchoring energy is calculated in the generalized Rapini-Papoular approximation

$$F_s = -\frac{1}{2}\int W_{ij}\,n_i\,n_j\,dS\ , \qquad (4)$$

where W_{ij} is the symmetrical anchoring tensor, that describes the pretilt angle as well as polar and azimuthal anchoring coefficients.

We study structures, which are periodic in the plane of the cell. Therefore, we simulate one unit cell in x and y directions, both in the plane of the cell, with periodic boundary conditions:

$$\mathbf{n}(\mathbf{r}) = \mathbf{n}(\mathbf{r} + \Lambda_x\mathbf{i}) = \mathbf{n}(\mathbf{r} + \Lambda_y\mathbf{j})\,. \qquad (5)$$

The discretized free energy $f = \frac{F_{FO} + F_s}{\Lambda_x \Lambda_y}$ per unit area (derivatives in each rectangular unit are substituted by corresponding differences between opposite faces of this unit) should have minimum with respect to $\mathbf{n}$ and maximum with respect to V. Therefore the relaxation to the equilibrium state is provided by the following 'motion' equations:

$$\gamma \frac{d\mathbf{n}_{\{m\}}}{dt} = -\frac{\delta f}{\delta \mathbf{n}_{\{m\}}}, \tag{6a}$$

$$\eta \frac{dV_{\{m\}}}{dt} = \frac{\delta f}{\delta V_{\{m\}}}, \tag{6b}$$

where the phenomenological viscosities γ and η are being adjusted during the calculation for the fastest convergence.

The free energy f per unit area of the cell reads as the quadratic form

$$f = f_0 + \sum_{\alpha=x,y} f_\alpha q_\alpha + \sum_{\alpha=x,y} f_{\alpha\beta} q_\alpha q_\beta, \tag{7}$$

where $q_{x,y} = 1/\Lambda_{x,y}$, f_α and $f_{\alpha\beta}$ are coefficients independent on q_α, so the extremum of f with respect to q_x and q_y is easily calculated after each step. This convergent process allows us to find both the free energy extremum and the periodicity of equilibrium state (Λ_x and Λ_y) simultaneously.

3. EXPERIMENTAL

We used chiral mixture E7 ($\varepsilon_\perp = 5.2$, $\varepsilon_a = 13.8$) doped with chiral agent CB15 (twisting power - $8\mu m^{-1}$), both purchased from EM Industries, Inc. A fluorescent Rhodamine 590 dye was added ($0.01 - 0.05$ wt%) to the cholesteric mixture for confocal-microscopy studies. LC cells with planar anchoring were assembled from two glasses coated with an ITO and polyimide aligning layers. Unidirectional buffing of the alignment layer set in-plane homogeneous orientation. Measurements in similar nematic cells with planar anchoring show[11] that the pretilt angle is in

the range $\theta_{pretilt} = 0 - 5°$ and the polar anchoring coefficient $W_p \sim 10^{-4} J/m^2$. Homeotropic anchoring was achieved by using lecithin alignment layers. Thickness of the liquid crystal slabs was set by spacers in the range from $1.5\mu m$ to $20\mu m$.

Olympus Fluoview fluorescent confocal microscope was used to study the internal structure of modulated states. Light from Ar^+ laser excites the dye molecules within the sample and the dye fluoresces. The feature of the confocal microscopy is extremely narrow depth of focus ($\sim 1\mu m$). It allows to scan horizontal slides of the LC, located at different depths in the bulk of the cell. As a result, the symmetry of director configurations can be reconstructed not only in the plane of the cell (as in usual optical microscope) but also in the plane normal to the slab.

4. RESULTS AND DISCUSSION

4.1. Planar cells.

The results described below were obtained for a cell with $p = 5\mu m$ and $d = 5 \pm 0.2\mu m$ ($d/p \approx 1$) and anti-parallel easy axes on the bounding plates. In zero field the texture is uniformly planar with small number of defects whereas in the strong field ($V > 5\,V$) it changes to a homogeneous conical (almost homeotropic) texture. Two kinds of modulated patterns are observed for the intermediate voltages (Fig.1), that differ both in the scenario of appearance and in orientation with respect to the rub direction:

(I) the stripes parallel to rub direction initially *nucleate* near spacers and other defects as circular zones; then these stripe elongates along the rub direction filling the available space;

(II) modulations perpendicular to the rub direction appear simultaneously all over the domain. These modulations develop by enhancing the optical contrast rather than by propagation in space.

We will refer to modulations (II) as 'developable' modulations to distinguish them from 'growing' modulations (I). Domains of developable and growing modulations can co-exist, Fig. 1. By changing the applied voltage, it is possible to move the boundary between two domains either way.

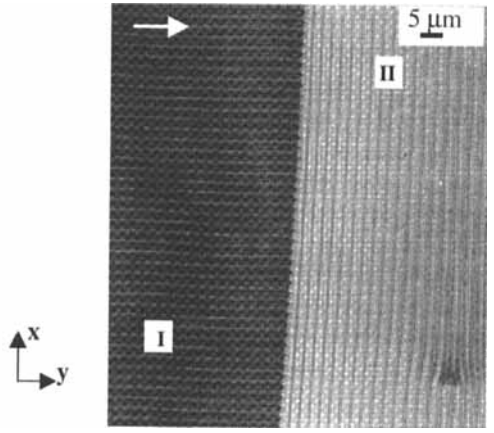

FIGURE 1. Polarizing microscope picture of growing (I) and developable (II) modulations. The horizontal arrow shows the rub direction. Note that the stripes in co-existing domains are perpendicular to each other.

(I) Growing stripes. Confocal image and computer simulated structure for growing stripes are shown in Fig. 2. For better resolution the images were obtained for a cell with a higher pitch ($p = 10\mu m$) but with the same ratio $d/p \sim 1$. In the bulk (middle of the cell), the structure is similar to the ideal cholesteric helicoid with the periodicity $p/2$, but interaction with surfaces breaks the symmetry between two adjacent stripes, so that the real periodicity doubles and becomes approximately equal to the pitch[7]. The difference between two adjacent stripes is clearly visible on the vertical cross-section of confocal microscope image (Fig.2a) and is reproduced by computer simulations (Fig.2b). The switching time from modulated to homeotropic state is about 10-40 ms, depending on the applied voltage. The reverse transition from homeotropic to modulated state, as well as transitions between planar and modulated states are rather slow (switching times ~ 0.1-1 s).

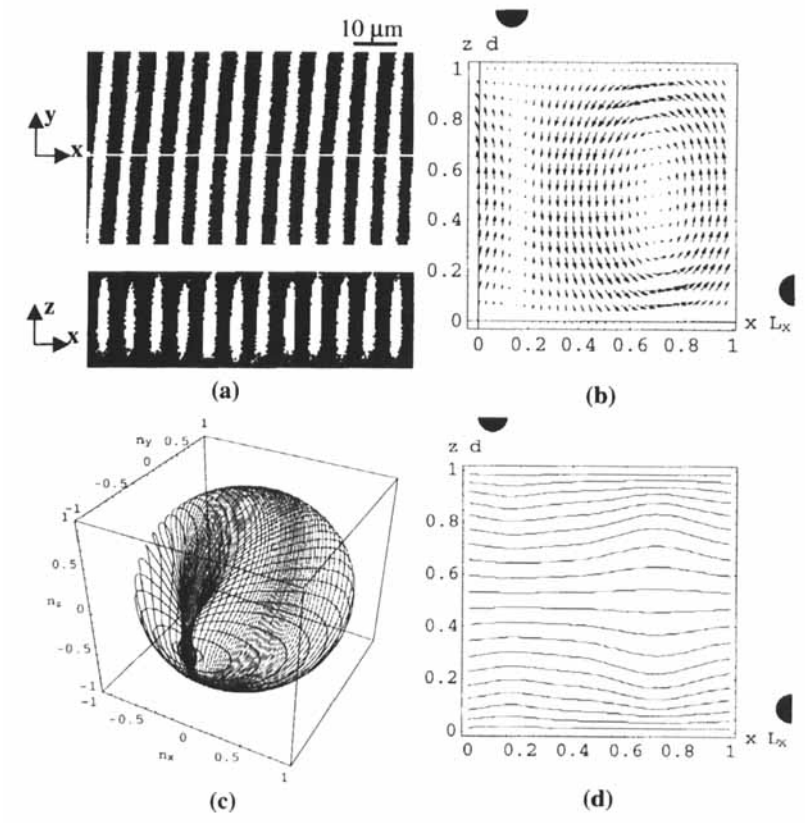

FIGURE 2. Confocal microscope image (a) and computer simulations (b-d) of growing stripes (I) in a cholesteric cell. Computer simulations (director field (b), S^2 representation (c), equipotential lines (d)) use the following parameters: K_{11} = 6.4, K_{22}=3, K_{33}=10 and K_{24}=0 (in 10^{-12} N); $\varepsilon_{\perp} = 5.2$, $\varepsilon_a = 13.8$; the cell has unidirectional planar boundary conditions ($\theta_{pretilt} = 3°$, $W_p d / K_{33} = 40$, $W_a d / K_{33} = 20$); applied voltage $U = 1.7$ V. The bounding substrates are normal to the axis z and the rub direction is along the axis y.

To clarify the director structure, we also use S^2 representation[12], in which $\mathbf{n}(\mathbf{r})$ maps the point of the surface $(0,L_x)\times(0,d)$ into the order parameter space S^2 (we neglect factorization $\mathbf{n}\equiv-\mathbf{n}$ for clarity of the pictures). In Fig.2c, the lines on S^2 correspond to the real-space scans along the x direction for different $z=const$. Note that Fig.2c clearly illustrates the tendency to form a double-twist structure.

(II) Developable modulations are shown in Fig. 3. These modulations appear as a result of dielectric instability similar to the Helfrich – Hurault instability in multi-layered ($d/p>>1$) systems. S^2 representation (Fig.3c) of these modulations is a result of expansion of the equator line, which corresponds to the planar state. Computer simulations (Fig.3b) allow one to interpret the features of the confocal image (Fig.3a). The difference of two adjacent dark bands is caused by non-zero pretilt angle. The two adjacent bright bands are different because of the lack of mirror symmetry (with respect to the middle plane of the cell) combined with the dye-induced absorbance. The switching times of developable modulations (II) (for a planar-modulated transition $\tau_{P\text{-}M}$ ~ 40 ms, for a modulated-planar $\tau_{M\text{-}P}$ ~ 80 ms) are smaller than those for growing stripes (I).

4.2. Homeotropic cells.

Modulated states with beam-steering effect can also be created in cells with homeotropic anchoring. The possible advantage is that in this geometry the modulations are stable in zero-field. The uniformity of modulations was set by an in-plane magnetic field; the modulations were preserved even when the magnetic field was switched off (Fig.4a). Applied electric field changes the details of director configuration and at high voltage transforms it into a pure homeotropic structure. Figure 4(b) shows computer-simulated zero-field state for homeotropic anchoring. The simulated structure reproduces correctly the diamond shape of stripe's vertical cross-section on the confocal image and even the diamond distortion. The structures are similar to the singular fingers CF-1[13], observed near the transition to the homeotropic state.

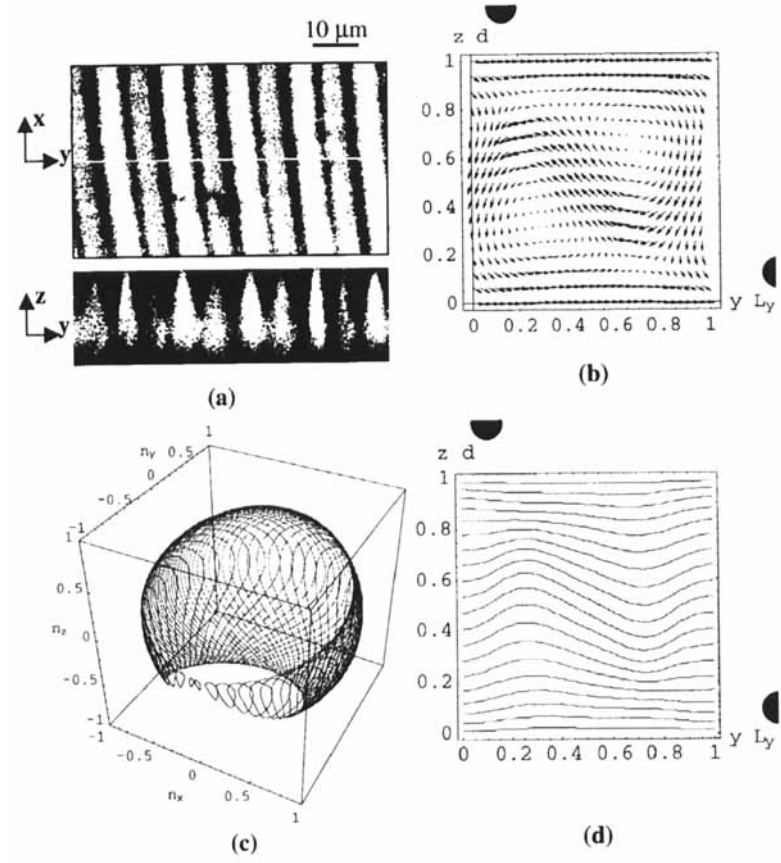

FIGURE 3. Confocal microscope image (a) and computer simulations (b)-(d) of developable modulations (II) in a cholesteric cell. Computer simulations (director field (b), S^2 representation (c), equipotential lines (d)) use the same parameters as in Fig.2; applied voltage $U = 1.8\,\mathrm{V}$. The bounding substrates are normal to the axis z and the rub direction is along the axis y.

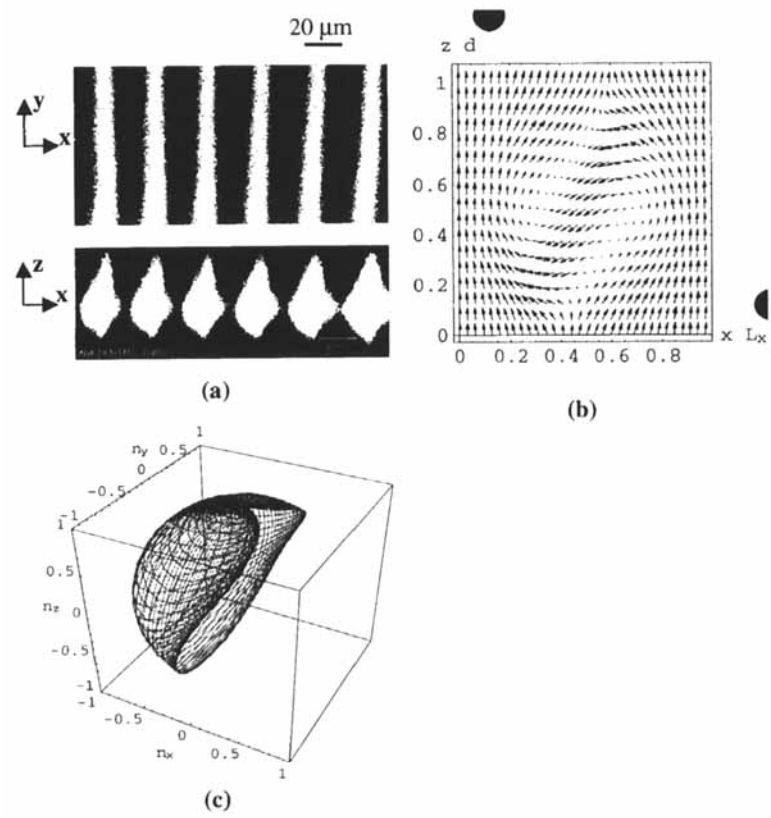

FIGURE 4. Confocal microscope image (a) and computer simulations (b)-(c) of homeotropic stripes in a cholesteric cell. Computer simulations (director field (b), S^2 representation (c)) use the following parameters: $\varepsilon_{\perp} = 5.2$, $\varepsilon_a = 13.8$ elastic constants $K_{11} = 6.4$, $K_{22} = 3$, $K_{33} = 10$ and $K_{24} = 0$ (all in 10^{-12} N); the cell has homeotropic boundary conditions ($W_p d / K_{33} = 10$), no applied voltage. The bounding substrates are normal to the axis z.

The switching time from the modulated (zero-field) to the homeotropic state (Fig.5) depends on applied voltage and the cell thickness and varies from 5 msec (for $U = 5\,\mathrm{V}$) to 40 msec (for $U = 1.2\,\mathrm{V}$, which is near the threshold voltage). The reverse transition from homeotropic to modulated state is rather slow (~ 0.1 sec). S^2 representation (Fig.4c) shows that these modulations can be developed from homeotropic state (the pole) smoothly and reversibly. However, the step-wise function of the switching time (Fig.5) indicates that dynamics of this transition is not simple.

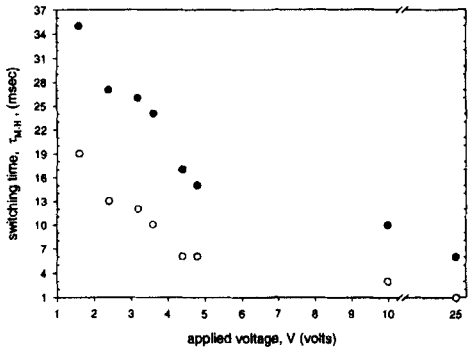

FIGURE 5. Switching time of M-H transition vs. applied voltage for cells with different thicknesses d (closed circles: $d = 5.0\mu m$, open circles: $d = 1.9\mu m$). Both cells have the same structures (homeotropic anchoring, d/p ~1).

CONCLUSION

We demonstrated that there are two different scenarios to form a CDG, a one-dimensionally modulated director configuration in the plane of a cholesteric cell, subjected to the external electric field. The first scenario is a first-order nucleation process with subsequent elongation of 'stripes'. The second process is a continuous (second-order) undulation-like instability in which the whole area of the cholesteric cell becomes

modulated when the voltage is high enough to tilt the director away from its original horizontal orientation. The second process is usually faster that the first one due to the absence of an energy barrier. The differences between two types of process are clearly revealed by comparing the details of director field in computer simulations and confocal microscopy, and through S^2 representation.

ACKNOWLEDGEMENTS

This work was supported by BMDO/AFOSR, Grant # F49620-96-1-0449 and by NSF ALCOM Center, Grant DMR 89-20147.

References

[1] P.F. McManamon, T.A. Dorschner, D.L. Corkum, L.J. Friedman, D.S. Hobbs, M. Holz, S. Liberman, D.P. Resler, R.C. Sharp, and E.A. Watson, *Proc. IEEE,* **84,** 268 (1996).
[2] K.M. Johnson, D.J. McKnight, and I. Underwood, *IEEE J. Ouant. Electron.* **29,** 699 (1993).
[3] J. Chen, P. J. Bos, H. Vithana, and D. L. Johnson, *Appl. Phys. Lett.* **67,** 2588 (1995).
[4] D.P. Resler, D.S. Hobbs, R.C. Sharp, L.J. Friedman, and T.A. Dorschner, *Opt. Lett.* **21,** 689 (1996).
[5] Zh. He, T. Nose, S. Sato, *Opt. Eng.* **37,** 2885 (1998).
[6] J. E. Stockley, D. Subacius, S. A. Serati, *Proc. SPIE* **3635,** 127 (1999).
[7] D. Subacius, Ph. Bos, and 0. Lavrentovich, *Appl. Phys. Lett.* **71,**1350 (1997).
[8] D. Subacius, S. V. Shiyanovskii, Ph. Bos, and 0. D. Lavrentovich, *Appl. Phys. Lett.* **71,** 3323 (1997).
[9] S. V. Shiyanovskii, D. Subacius, D. Voloschenko, Ph. Bos, and 0. D. Lavrentovich, *Proc. SPIE,* **3475,** 56 (1998).
[10] O. D. Lavrentovich, S. V. Shiyanovskii, and D. Voloschenko, *Proc. SPIE,* **3787**, 149 (1999).
[11] Yu.A.Nastyshyn, R.D. Polak, S.V. Shiyanovskii, O.D. Lavrentovich. *Appl. Phys. Lett.* **75,** 202 (1999).
[12] F.Lequeux, *J. Phys. France* **49**, 967 (1988).
[13] J. Baudary, S. Pirkl, P. Oswald, *Phys. Rev. E* **53,** 3038 (1998).